LA-UR--89-300

DE89 006560

Los Alamos National Laboratory
Los Alamos, New Mexico

DIRECT LASER MATERIALS INTERACTION LASER ABLATION OF SUPERCONDUCTOR MATERIALS AND LASER WELDING

D A Cremers[a] R D Dixon[b] R C Estler[c] G K Lewis[b] J L Lyman[a] R F Muenchausen[d] N S Nogar[e] and M Pitch[f]

RUNNING HEADING Direct Laser Materials Interaction

ABSTRACT

This paper considers two applications of direct laser materials interaction, laser ablation of superconductor materials and Nd YAG laser welding The laser ablation experiments with 355 nm, 10 ns pulses have demonstrated uniform thin superconductor films The film uniformity was improved significantly be rotating both the laser target and the film support and by vertically dithering the laser focus The film stoichiometry does vary with laser fluence but it is within 10% of the target material at high fluence Annealing of the thallium containing films restores lost oxygen For the welding application we have investigated the conditions that influence the melt depth High speed photography has shown the plume to consist of a series of regenerated pulses that move in a direction normal to the surface The time for plume initiation and the laser power threshold for plume formation are dependent on the substrate material The plume temperatures depended on the welding atmosphere Temperatures and melt depths are higher for the reactive gases air O_2 and SF_6 than for the nonreactive gases He Ar and N_2

[a] Mr. [illegible] Los Alamos National Laboratory Los Alamos NM 87545

[b] Mr. [illegible] Los Alamos National Laboratory Los Alamos NM 87545

[c] Dept. of Chemistry Fort Lewis College Durango Colorado 81301

[d] Mr. [illegible] Los Alamos National Laboratory Los Alamos NM 87545

[e] Dr. [illegible] Los Alamos National Laboratory Los Alamos NM 87545

[f] Mr. [illegible] Los Alamos National Laboratory Los Alamos NM 87545

Table 1 Parameters

Laser ablation experiments for thallium containing superconductor films laser welding experiments stainless steel

INTRODUCTION

Processes as diverse as welding and production of superconductor films may take advantage of the unique properties of laser radiation. This paper reports the results of research in each of these two areas: (1) the production of thallium containing high temperature superconducting thin films by laser ablation and (2) laser welding. The first application requires short laser pulses (~10 ns) and the second much longer pulses (~8 ms). Consequently, the conditions under which the irradiated material absorbs the laser radiation are quite different. For the ablation process the local pressure during and shortly after the laser pulse may greatly exceed ambient. This results in the near explosive removal of the material in the irradiated region. The welding laser, on the other hand, heats the material slowly enough that acoustical processes keep the pressure in the irradiated region close to ambient. The welding laser does form an evaporative plume, but it results from slow evaporation, not an explosive expansion.

Laser welding is a well developed technology. The objective of the research at Los Alamos is to develop sufficient understanding of the laser interaction process to bring more versatility to the technique. Laser ablation of superconductor materials is only a recent development. Our goal again is to increase understanding of the process. We wish to find conditions where the stoichiometry is preserved and the deposited films are of high quality.

LASER ABLATION OF SUPERCONDUCTOR MATERIALS

Applications of the new metal oxide based perovskite high temperature superconductors (HTSCs) are dependent, in many instances, upon the ability to fabricate superconducting thin films. A number of approaches, including sputtering, co-evaporation and ion assisted deposition, employing both elemental and compound sources, have been used to produce high quality HTSC thin films.[1] One difficulty with elemental sources is that the relative evaporation rates for each source must be kept constant throughout the deposition by independently varying the temperatures and/or sputter rates. On the other hand, compound sources often suffer from the fact that the various metals and their oxides have significantly different vapor pressures and ion and electron sputter yields. The final composition of the film will also depend on process variables such as background pressure, deposition rate, etc.

Laser deposition can reduce or circumvent a number of these difficulties[illegible]. A single source may be used, obviating the need for multiple deposition rates control. In addition, the rapid energy deposition possible with laser sources results in temperature rises so rapid [illegible] that congruent evaporation can occur without significant elemental fractionation. In addition, laser evaporation can be used under a variety of processing conditions: deposition pressure may vary from UHV to several torr of inert or reactive atmospheres, and deposition temperatures are restricted only by the physical properties of the target and substrate materials used.

A number of groups have demonstrated deposition of metal oxide thin films[illegible] using Nd:YAG[4], excimer[illegible] and CO_2[illegible] lasers. The majority of this work has been done with YBaCuO systems[4-illegible], though more recently some work has been done on Bi-Sr-Ca-Cu oxide systems[8].

We have recently demonstrated[9] the production of superconducting $YBa_2Cu_3O_{7-x}$ films using the Q-switched third harmonic (355 nm) output from a Nd:YAG laser. Third harmonic radiation was used in preference to 1.06 μm or 532 nm because of the large absorption coefficient, shallow penetration depth and relative immunity from both slow thermal processes and particulate formation in the film at this wavelength[illegible]. More recently, we have turned our attention to the deposition of thallium containing thin films because of the more desirable chemical, physical and electrical properties of these superconductors[illegible]. We will describe recent results on deposition conditions, plume diagnostics and film properties resulting from deposition at 355 nm from both 2122 and 2223 thallium calcium barium copper oxide targets.

Experimental

Films were deposited in a [illegible] of stainless steel conflat six-cross with an additional port on one [illegible] for optical access, as shown in Fig. 1. Pressures during deposition were typically maintained at a few [illegible] torr by an oil free mechanical pump. Bulk samples [illegible] diameter were mounted on a vacuum feedthrough and rotated at [illegible] rpm in order to assure even deposition. The substrate, located [illegible] from the target, was also rotated at a comparable rate in the opposite direction. The substrate can be heated by a quartz lamp mounted [illegible] to temperatures of [illegible]. [illegible] The deposition temperature used in these experiments was typically between [illegible]

Laser pulses of 15-25 mJ at 355 nm were generated by frequency tripling the Q-switched output [illegible] ns from a Nd:YAG laser equipped with filled beam optics. Mild focusing produced a fluence at the sample surface of 1-15 J/cm^2 and a confocal parameter much larger than the etch depth in these experiments. The laser was operated at 10 Hz and deposition times were from 15-90 minutes. The final turning prism was dithered vertically at 0.1 Hz in order to etch the target surface evenly.

As deposited films were insulating and required a post deposition anneal at 850^{o} C for 15 minutes in a [illegible]-enriched crucible to compensate for [illegible] loss from the film. Subsequent annealing at 750^{o} C in an O_2 atmosphere for 2-8 hours gave shiny, black films with room temperature resistances between 100-500 Ω.

Results

Most evaporations utilized a laser fluence in the range 4-7 J/cm^2. Dithering the steering prism resulted in a circular etch pattern covering most of the target surface, as seen in Fig. 2. This proved to be far superior to etching a single track at fixed radial distance, which resulted in severe spatial distortion of the emitted plume, as well as thickness and compositional variations in the films. Consequently, a more reproducible deposition rate was obtained as evidenced by Fig. 3, which shows a plot of film thickness as a function of deposition time for subsequent runs. The film thickness for the rotated substrates as measured with a stylus profilometer was uniform to [illegible] 10% over the area coated [illegible] 0.5 cm^2. This was a factor of two better than obtained for unrotated substrates.

During the deposition process, [illegible] ng/pulse was typically removed from the bulk target, and only [illegible] ng/pulse deposited on the substrate. This corresponds to a deposition rate between 1-5 Å/s. The difference between the etch rate and the deposition rate was presumably due to a combination of imperfect overlap of the ablation plume with the substrate, non-unity sticking coefficient and, perhaps, gas phase reactions occurring prior to impact on the substrate. Empirically, the deposition rate was found to vary with target composition, grain size, sintering process, length of previous exposure, and length of time between target synthesis and exposure to the laser. [illegible] From our correlated film thickness [illegible] and exposure geometry, we deduce [illegible] [illegible] which is consistent with [illegible]

[illegible]

[illegible]

[illegible]

355 nm, as shown in Fig. 4. For both wavelengths, the films were found to be deficient in calcium and enriched in Tl relative to the starting material near the threshold fluence for deposition. Although this result can not be explained in terms of simple volatility or reactivity arguments, it is consistent with recent observations on [illegible] laser evaporation of the similar Bi-Ca-Sr-Cu-O films. In our experiments, the stoichiometry approached that of the starting material as the fluence was increased. At five times the threshold fluence, the film deposition was stoichiometric (within [illegible]) to that of the target material. At higher fluences, the composition is then relatively independent of fluence over a broad range. An upper limit on useable fluence is imposed at [illegible] J/cm^2 by the deposition of relatively large particulates [illegible] as shown by scanning electron microscopy (SEM).

The as-deposited [illegible] films were invariably deficient in oxygen and required a post-deposition anneal, as described above. In order to develop an in situ deposition process, we are investigating a number of diagnostics on the laser generated plume, including optical emission and mass spectroscopy. Representative mass spectrometry results are shown in Fig. 5, which shows both the dynamic range available in our measurements, and some interesting aspects of the evaporation process. In particular, no BaO ions are visible in this spectrum. We were also unable to detect any oxide ions containing [illegible] in the plume. On the other hand, we were able to detect large quantities of both neutral and ionic oxygen atoms and molecules. This suggests that the evaporation process is sufficiently violent that the metal oxide bonds are dissociated. The higher volatility and reactivity of the oxygen species, relative to metal atoms and ions, suggests an explanation for the lack of oxygen in the as-deposited films relative to the target.

[illegible]

Laser evaporation at 355 nm has been demonstrated to produce [illegible] that [illegible] the bulk under mild processing conditions. [illegible] the laser beam across the target surface in combination with rotation of the target produces a much more uniform film than does simple target rotation. In addition, filtering of the laser beam external to the target chamber is more easily implemented than placing [illegible] within the deposition chamber and [illegible] improves the deposition [illegible] reproducibility. [illegible] deposition of thallium containing thin films is more difficult than [illegible]

high volatility of thallium and its oxides. Future efforts in this laboratory will center on implementation of an activated oxygen source in an attempt to lower the processing and/or annealing temperatures required.

LASER WELDING

In the laser welding process, the laser is used as a source of energy that heats the substrate material above its melting point to produce a fusion weld. However, the process is complex because of interactions between the laser beam and the material that may either increase or decrease the coupling of energy into the weld.[6,7] During the melting process a fraction of the incident laser energy is absorbed by the substrate. The remainder is reflected or absorbed above the surface by the plume, which forms if the surface temperature is sufficiently high. The plume consists of evaporated metal, hot atmospheric gases, and reaction products. At low laser power heating of the bulk metal is by thermal conduction from the laser heated surface (conduction mode). At higher laser power a vapor depression may form in the melt pool, which may greatly enhance both the energy coupling and the melt depth. This process is called keyhole formation[8] (keyhole mode). Other processes that influence the energy coupling include absorption of laser radiation by the plasma or plume, convection in the weld pool, reflection from the surface of molten metal, chemical reactions in the plume or melt pool, scattering from particles in the plume, and defocusing effects caused by the changing index of refraction in the plume.

Control over the process depends on understanding the laser material interactions and the energy balance involved among these interactions. With this knowledge, process diagnostics and enhancement techniques can be developed.

Most Nd:YAG welding lasers are pulsed. Most CO_2 welding lasers are continuous wave. The time scales of events (melting, evaporation, thermal conduction) during the Nd:YAG pulse are generally shorter than the laser pulse length (~8 ms). From an energy coupling point of view, even the pulsed laser may be considered continuous wave. From the metallurgical viewpoint, however, (rapid heating, melting, cooling, and solidification) occurring with each pulse may produce different physical and mechanical properties compared to a continuous wave weld.

The major emphasis of the Nd:YAG laser welding research has been (1) to determine the [illegible] melt depth and (2) to develop real-time welding diagnostics. The experimental [illegible] were integrated light emission from the plasma and the plume temperature. The temperature [illegible]

was determined by atomic emission spectrometry and the melt depth by metallography. The experimental conditions evaluated include laser pulse energy, gas pressure, and gas reactivity. The melt depth was correlated with gas composition and oscillations in the plume height.

Experimental

The Nd:YAG laser used in the welding experiments had a maximum pulse energy of 40 J. The pulse rate for all experiments was 10 Hz and the pulse length was 1.8 ms. Careful measurements of the spot size showed that it varied somewhat with the pulse energy. At low pulse energy (10 J) it was 0.75 mm diameter and at 40 J it was 1.5 mm diameter. For some of the experiments we report the average laser power and for others the power density at the target during the pulse. For the former the pulse energy is obtained by dividing the average power by ten.

The high speed photography experiments were performed with a Spin Physics video camera that operated at [illegible] frames per second and 6 images per frame. Consequently, the time between individual images was 83 µs.

Figure [illegible] shows a diagram of the experimental layout for the spectroscopic experiments. The light from the weld plume was imaged onto the entrance slit of a 1.5 meter spectrograph; the spectrally dispersed light was detected by a time gated photodiode array. The array could be gated to monitor events occurring over an interval [illegible] µs in duration. Light from the plume and the laser pulse temporal profile were monitored using fiber optic cables and photomultiplier tubes. The output of the detectors was recorded on a digital oscilloscope.

[illegible] Plume Analysis

The characteristics of the plume produced by the laser will be influenced by several properties of the target. These include: the fraction of the incident laser beam absorbed (emissivity), the thermal conductivity, the enthalpy of vaporization, and the boiling point. The most important of these properties [illegible] [illegible] [illegible] [illegible]

[illegible] [illegible] [illegible] [illegible] The thermal

[illegible] [illegible] [illegible] [illegible] energy to the bulk metal. The

thermal conductivity of aluminum (3 W cm^{-1} K^{-1}) exceeds that of stainless steel (0.3 W cm^{-1} K^{-1}) by about a factor of ten.[8] Melting the metals significantly lowers the thermal conductivity.[11]

Figure 7 shows high speed photographs of the plume formation above individual spot welds made on 304 stainless steel (304SS) and commercially pure aluminum (1100 Al). These two materials were chosen to be representative of materials that highly reflect (Al) and highly absorb (SS) the 1.06 μm light from the Nd:YAG laser. Each horizontal panel shows a succession of individual photographs of the plume which expands vertically above a horizontal sample surface. Each panel corresponds to a weld made by one laser pulse. The time between successive photographs is 83 μs. The sample surface does not show in the photographs because the camera f stop was adjusted for proper exposure of the plume, which was much brighter. A fiducial mark shown as a white block to the left of each photograph sequence marks the start of the laser pulse. The powers used at the left are the average laser powers measured at a pulse rate of [illegible].

The temperatures of the weld plumes on 1100 Al and 304SS were measured using neutral iron lines in the spectral region [illegible]. The concentration of iron in 1100 Al is below 1%, so these lines are suitable to construct a Boltzmann plot to determine temperature. Figure 8 shows the temperature, as determined by atomic emission spectroscopy, at various times during the laser pulse. The laser pulse energy is the same ([illegible]) for both materials. The more strongly absorbing 304SS target gives a plume temperature that is several hundred degrees higher than the aluminum target.

The time to the initiation of the plume is shorter for 304SS than 1100 Al because of the greater absorption of the steel sample. Figure 9 shows the initiation time (measured from the photograph sequences) plotted versus average power. Plumes initiate at [illegible] W ([illegible]) average power on the [illegible] sample compared to [illegible] W ([illegible]) on the 1100 Al sample. [illegible] time for plume formation drops from [illegible] changing the power from [illegible] W [illegible] on the 1100 Al sample plume initiation [illegible] after [illegible] at [illegible] W [illegible] and dropped to [illegible] at [illegible] W [illegible]. The power [illegible] required for plume initiation is constant for a given surface condition, material, and atmosphere.

[illegible] of the plume will be influenced by the same material properties that determine the plume [illegible] average laser power of [illegible] W the initial stainless steel plume rises at a rate of [illegible] while the initial aluminum plume [illegible] same average laser power rises at a rate of [illegible].

Both of these rates are only a small fraction of the sonic velocity. For example, the rise rate for 304SS is 6.4% of the room temperature sonic velocity in air. The ratio of the rates for 304SS and 1100Al (3.7) is about the same as the ratio of emissivities (2 to 4) for these two materials.

At high powers the welding plumes for both materials tend to rise, expire, and reinitiates during the pulse. The occurrence of these oscillations appears to have an energy threshold and the number of pulses increases quickly for both materials with increasing power. Up to 22 plume pulses were counted on the 304SS sample and 18 on the 1100Al sample. Experiments with 5052 and 6061 aluminum showed similar effects. The threshold pulse energies appear to be the same for the three aluminum alloys, but the number of plume pulses for 5052 Al was about 2/3 that of the other alloys. The threshold energy for these plume pulses corresponds to a significantly increased melt depth and the onset of keyhole formation. The occurrence of the plume oscillations has been attributed[12] to successive opening and closing of the keyhole depression, that is, to oscillation of the melt pool.

Keyhole formation results in increased absorption because of multiple reflections of the incident laser radiation. In addition to the dramatic increase in melt depth, we also see that the rate of rise of successive plumes is greater than for the initial plumes. This is particularly true for Al 1100. For 370 W average power, the rate of rise of later plumes is three time that for the initial plume. We conclude, then, that the keyhole formation increases the fraction of the laser radiation absorbed by aluminum by about a factor of three.

Effect of the Welding Atmosphere on Melt Depth

The atmosphere above the melt pool is known to effect the welding process. For example, gases such as N_2 and H_2 in the cover gas during welding can be incorporated into the weld and lead to embrittlement. To study the effect of different gases on the weld depth, the workpiece was placed in a sealed chamber which was purged by different gases (Fig. 6). The melt depths obtained as a function of laser power [illegible] using various purge gases are shown in Figs. 10 and 11 for continuous welds on 1100Al and [illegible]. The welds were made at [illegible] Hz with [illegible] overlap between adjacent welds. The divergence [illegible] [illegible] during these experiments by adjusting the collimator [illegible] [illegible] was changed. [illegible] with the adjustment the spot [illegible] [illegible] the workpiece [illegible] with increasing laser power.

Two distinct regions are evident in Figs. 10 and 11: (1) At power densities below about 1.3 MW cm^{-2} there was a small but gradual increase in the melt depth with increased power density and (2) above 1.3 MW cm^{-2} there was 5-10 fold increase in the melt depth with a small increase in power density. Comparison of the figures in the low power regime shows that the melt depths in 304SS were about three times the melt depths in 1100Al at the same power densities. Also, for 304SS the slopes of the curves at low power density are about five times greater than those obtained for 1100Al. Both these effects may be indicative of the greater thermal conductivity and reflectivity of aluminum compared to stainless steel. Inspection of the figures also shows that at a specific power density, the welds made in air, O_2, and SF_6 were deeper than those obtained in the other gases. The greatest effects were for the 304SS welds in which melt depths in O_2 and SF_6 were 5.4 and 2.9 times, respectively, the depth obtained using He at a density of 1 MW cm^{-2}. In addition, the rates of change of melt depth with power density were greatest for the more reactive gases. These differences are attributed mainly to the different reactivities of the gases. As stated above, temperatures in the welding plume can reach 3500 K which is sufficient to generate free oxygen and fluorine atoms that can react with aluminum or iron to produce heat. The reaction 2Al + 3O = Al_2O_3, for example, is very exothermic with ΔH = 400 kcal/mole. The energy required to melt the volume of the largest melt produced in 1100Al (2 mm D x 1.8 mm W) is 3.23 J. This energy is generated if only 2% of the aluminum in the melt volume reacts to form the oxide. Similar results apply to the formation of iron oxides and fluorides. Measurements of the temperature of the plumes produced in the different gases are presented in Fig. 12. These data show that the temperature is greater for the reactive gases, suggesting that energy is being released via a reactive mechanism.

The increase in melt depth obtained with the reactive gases could also be due to greater coupling of the laser energy into the metal by formation of the oxides. Aluminum oxide, for example, exhibits much stronger absorption at 1.06 microns than pure aluminum metal. Other gas properties, such as thermal conductivity, may have a role in determining the melt depth but their effect is probably small. The thermal conductivities of O_2 and N_2, for example, are almost identical but significantly deeper melt depths were achieved in [illegible] Fig. 10. It is also possible that some as yet undetermined parameter of the welding process, for example, changes in the spot size due to thermal lensing in the different gases, may account for the observations reported here but these effects are expected to be small.

The curves in Figs 10 and 11 show that at powers above 1.3 MW cm^{-2} a new mechanism becomes operative in each gas that produces a significant increase in the melt depth. This dramatic increase in the weld depth at the higher powers is probably due to a change in the welding mode from conduction to keyholing in which the laser beam is effectively channelled into a vapor cavity within the melt via multiple reflections. In the keyholing mode, as noted in the previous section, the fraction of laser energy coupled into the metal increases significantly over that obtained in the conduction mode. The transition from conduction to keyhole mode is demonstrated in Fig. 13 which shows cross sections of welds made on 1100Al in argon and air at different laser powers. At 300 W, which corresponds to a power density of about 1.34 MW cm^{-2}, the weld profile corresponds to the conduction mode. At 350 W (1.36 MW cm^{-2}) the onset of keyholing is evident with a significant increase in the depth-to-width ratio of the weld. The main effect of the reactive gases over the transition region appears to be a slight reduction in the power density at which the transition from conduction to keyholing occurs. Unfortunately, it is not possible to increase the power density above 1.36 MW cm^{-2} to observe whether the large increase in melt depth with power continues at higher powers.

Conclusion

The properties of the welding plume correlate with the characteristics of a laser weld. A prompt initiation and rapid rise of the plume indicates effective coupling of the laser radiation to the workpiece. The plume oscillations are also indicative of operation in the keyhole mode. We now have sufficient data and understanding to begin the development of diagnostics based on plume properties that can be good indicators of weld characteristics. The studies with different atmospheric gases show the importance of gas-metal vapor reaction in determining the heat input to the weld. This gives another degree of freedom that one can use in controlling the weld properties. As this research continues, the development of a computer model of the welding process will become a high priority. The development of improved heat dissipation diagnostics, and the establishment of a more quantitative correlation between plume characteristics and weld properties is continuing.

ACKNOWLEDGMENTS

This work was performed under the auspices of the United States Department of Energy. The authors appreciate the support of the management of the Los Alamos National Laboratory during the course of this research.

REFERENCES

1. See for example Novel Superconductivity Wolf S A and Kresin V Z eds Plenum NY
2. Wu X D and Venkatesan T in Chemistry of Oxide Superconductors Rao C N R ed
3. Sankur H and Cheung J T Appl Phys A47 271 1988
4. Kwok H S Mattocks P Shi L Wang X W Wilamowski S Yang Q Y Cheung J D and Shaw D T Appl Phys Lett 52 1825 1988
5. Wu X D Dijkkamp D Ogale S B Inam A Chase E W Miceli P F Chang C C Tarascon J M and Venkatesan T Appl Phys Lett 51 861 1987
6. Dijkkamp D Venkatesan T Wu X D Shaheen S A Jisrawi N Min-Lee Y H McLean W L and Croft M Appl Phys Lett 51 861 1987
7. Roas B Schultz L and Endres G Appl Phys Lett 53 1557 1988
8. Jagga N K Meskoob M Wahid S F and Rollins C J Appl Phys Lett 53 1951 1988
9. Garcia A R Mueller-Lierau R T Nagar N S unpublished results
10. Vaught A W Nature 242 1973 1988
11. Venkatesan T Wu X D Inam A and Wachtman J B Appl Phys Lett 52 1193 1988
12. Thompson J "The influence of laser induced plasma on laser materials processing" in The Industrial Laser Annual Handbook Pennwell Publishing p 108
13. Pirri A N Root R G and Wu P K S "Plasma energy transfer to metal surfaces irradiated by pulsed lasers" AIAA Journal 16 1296 1978
14. "The Physical Properties of Liquids at Elevated Temperatures" in The Physics of Welding Pergamon Press 1986 p 9
15. Goldston R B Plasma Physics and Magnetic Fluidmechanics McGraw Hill 1984
16. "Laser Beam Welding" Metals Handbook 9th Ed American Society for Metals p
17. Thermophysical Properties of Matter Vol 7 Thermal and Radiative Properties Metallic Elements and Alloys 1970
18. Handbook of Chemistry and Physics 69th Edition CRC Press Inc Boca Raton Florida 1988

FIGURE CAPTIONS

1. A schematic of the experimental apparatus. The target and substrate are rotated at [illegible] rpm while the laser beam is rastered at [illegible]. Typical pressures in the deposition chamber were [illegible] $10^{-[illegible]}$ torr.

2. A micrograph ([illegible]) of the laser etched (dark) and unexposed (bright) parts of the target pellet. The grains observable at the etched part of the pellet are characteristics of the starting material. The unexposed area is brighter due to a [illegible] formed during final sintering of the pellet.

3. Shows deposition thickness of the thin film (in kÅ) vs deposition time at constant fluence and repetition rate. This indicates that a constant amount of material is being deposited with each laser shot.

4. The film composition (determined by Rutherford backscattering spectrometry) as a function of [illegible] for [illegible] irradiation (open symbols) and 532 nm irradiation (filled symbols).

5. Mass spectrum of the ablated plume showing dynamic range and sensitivity of the measurement for [illegible] and the [illegible] detectable metal oxide.

6. Apparatus diagram for the laser welding experiments.

7. High speed photographs of the rising plume during a single Nd:YAG laser pulse. Time increases to the right and the time between images is 8 [illegible]s. The label on the left margin is the average laser power [illegible]. The highest [illegible] are [illegible] cm for [illegible] and 1.25 cm for [illegible]Al.

8. Temperature [illegible] versus time during a [illegible] laser pulse for two different materials.

9. [illegible] for initiation of laser plume versus average laser power for [illegible] and several aluminum alloys.

10. Melt depth in [illegible] versus laser power density for six different atmospheres ([illegible] torr) from a series of overlapping laser pulses.

11. Melt depth in [illegible]Al versus laser power density for six different atmospheres ([illegible] torr) from a series of overlapping laser pulses.

12. Melt depth for continuous welds in [illegible]Al versus temperature of the laser plume. The laser power was the same for all points. The temperature variation was produced by varying the gas over the weld. [illegible] the left the gases were N_2, Ar, Air, [illegible], and [illegible].

13. Weld profiles for two different gases for three different laser powers that span the [illegible] of [illegible] formation.

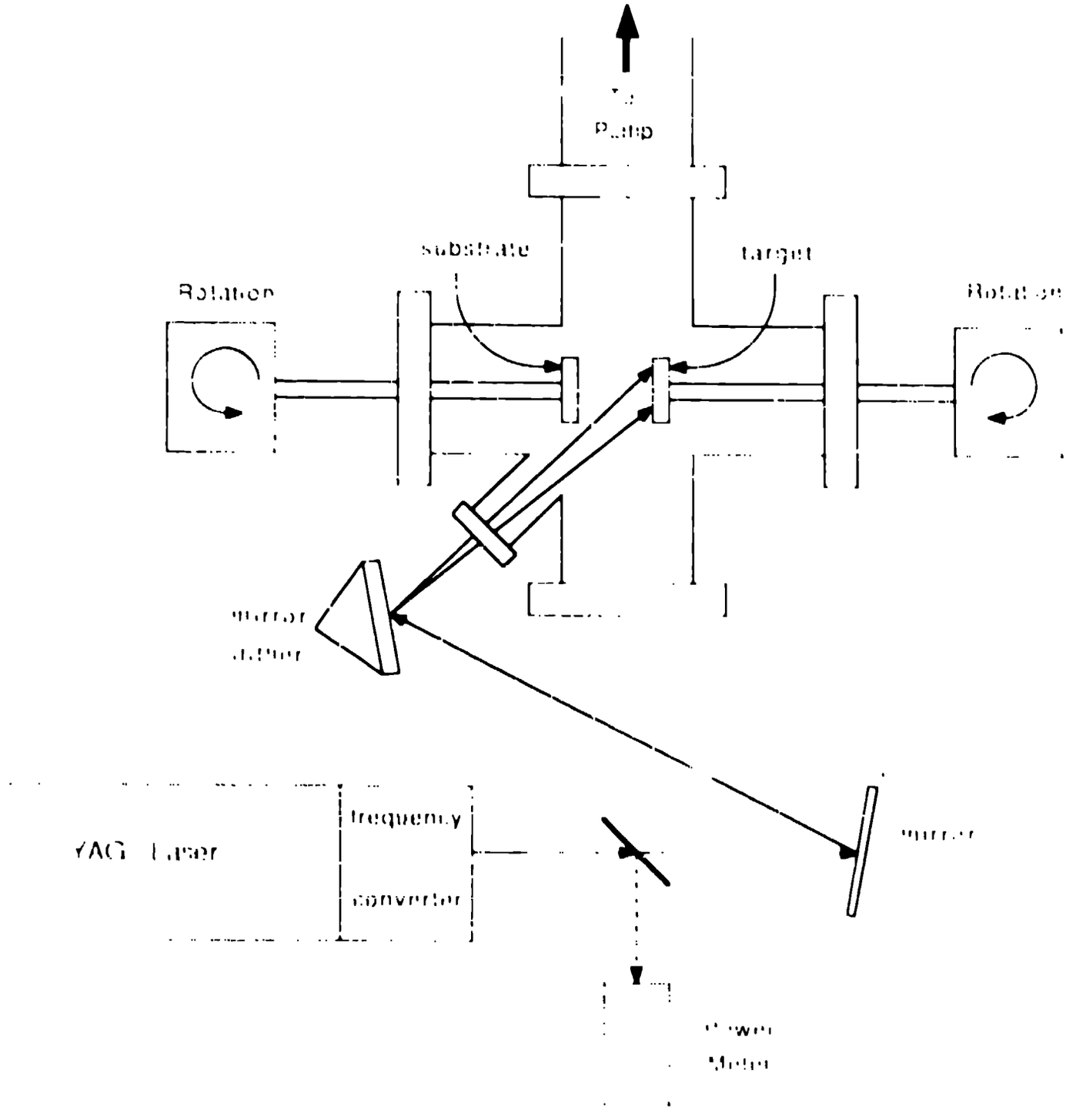
substrate
target
Rotation
mirror
frequency
converter
mirror

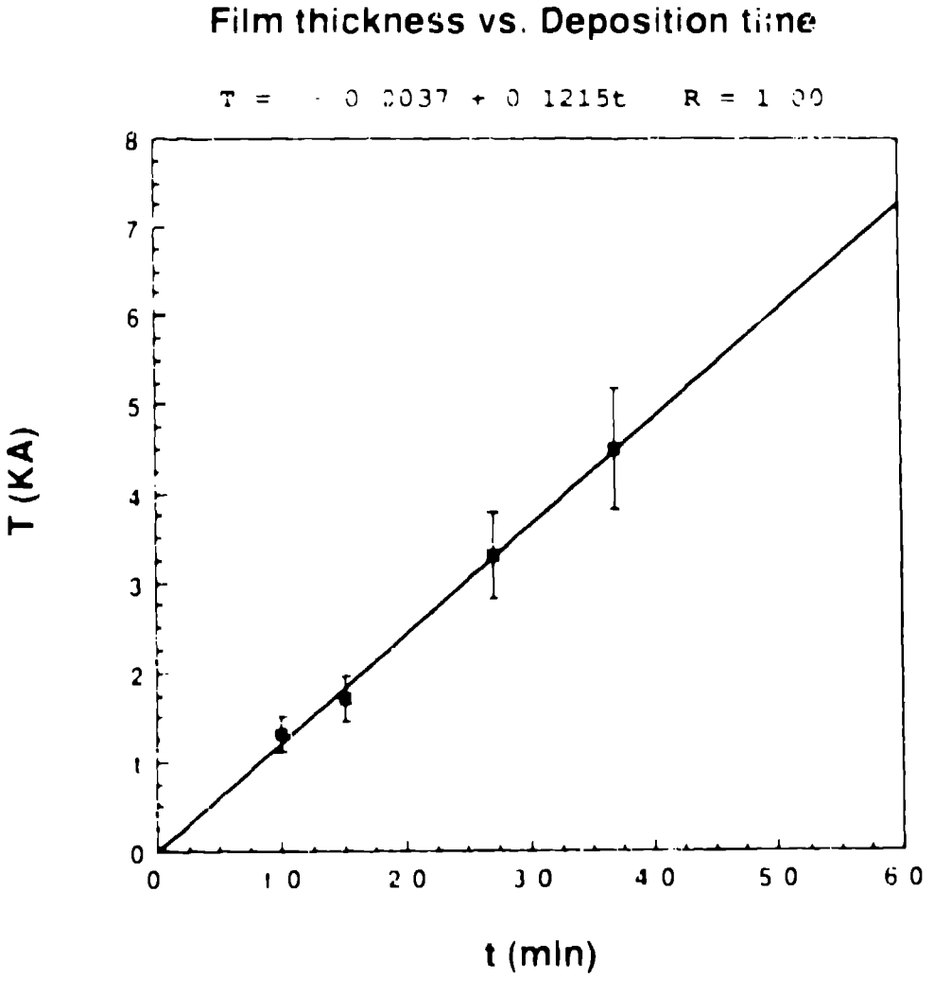
Film thickness vs. Deposition time
T = - 0 0037 + 0 1215t R = 1 00
T (KA)
t (min)
0
1
2
3
4
5
6
7
8
0
10
20
30
40
50
60

Figure 1

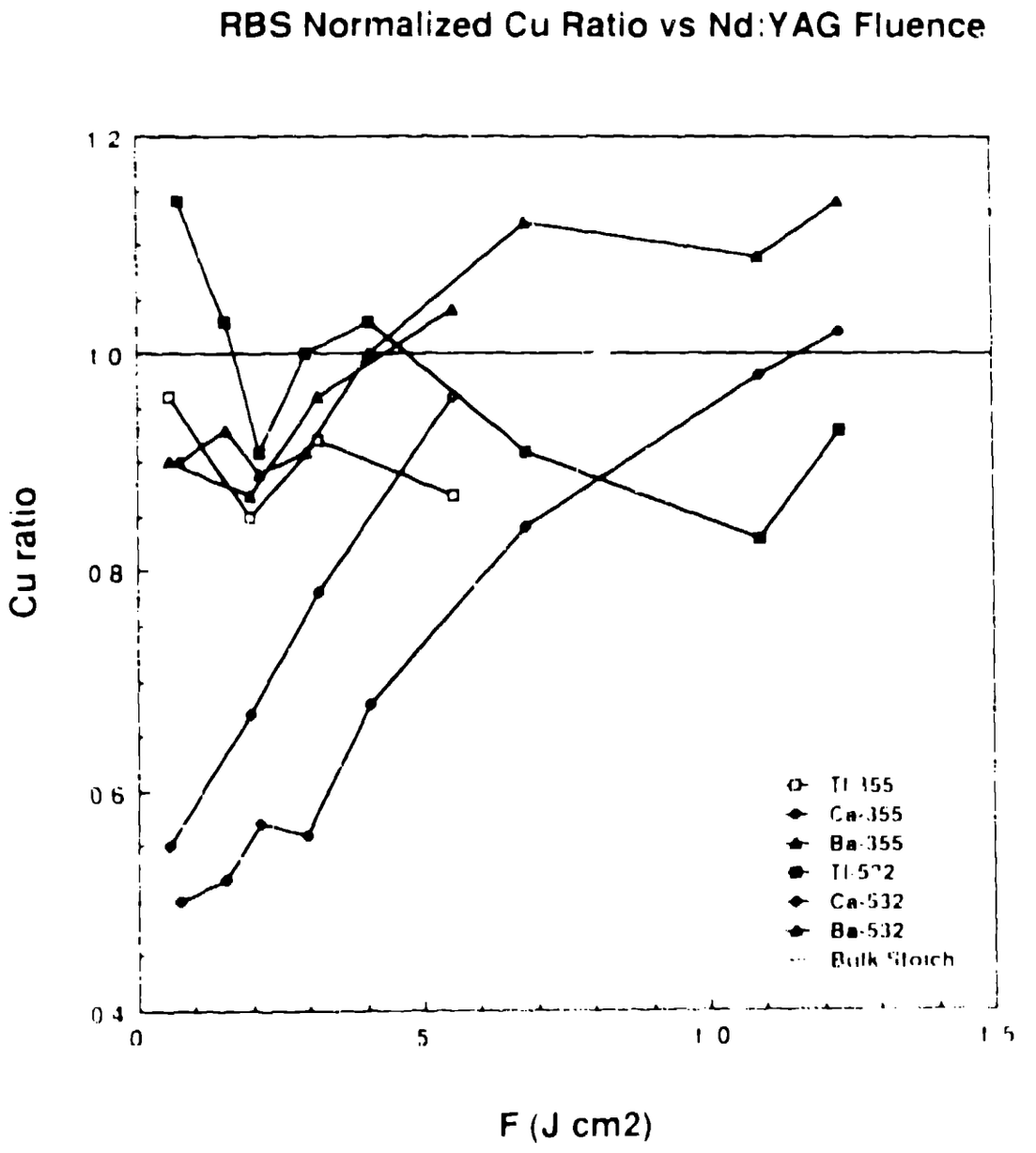
RBS Normalized Cu Ratio vs Nd:YAG Fluence
Cu ratio
1.2
1.0
0.8
0.6
0.4
0
5
10
15
F (J cm2)
Tl-355
Ca-355
Ba-355
Tl-532
Ca-532
Ba-532
Bulk Stoich

Figure 4

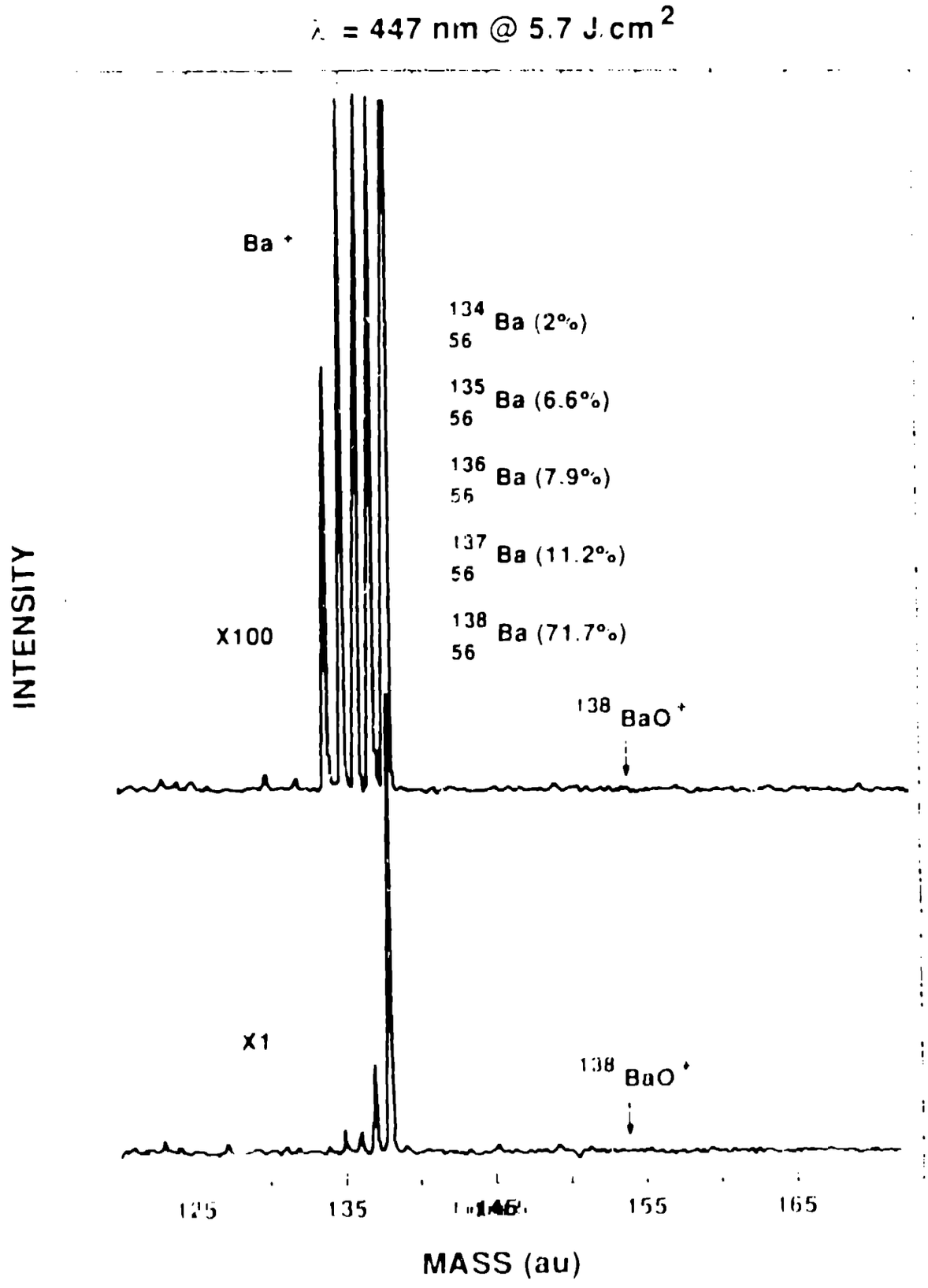
λ = 447 nm @ 5.7 J/cm²
Ba⁺
¹³⁴₅₆Ba (2%)
¹³⁵₅₆Ba (6.6%)
¹³⁶₅₆Ba (7.9%)
¹³⁷₅₆Ba (11.2%)
¹³⁸₅₆Ba (71.7%)
X100
¹³⁸BaO⁺
X1
¹³⁸BaO⁺
INTENSITY
125
135
145
155
165
MASS (au)

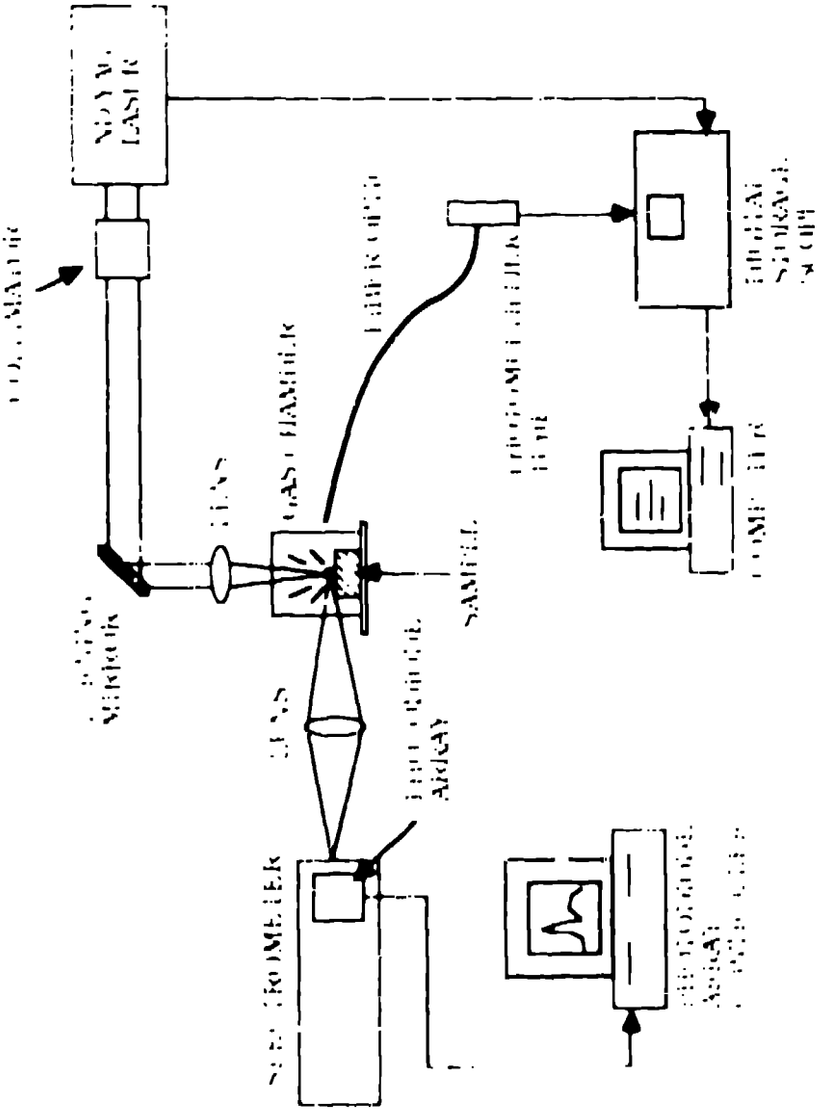

Figure 6

Nd - YAG LASER PLUMES

304SS (7ms, 10pps)

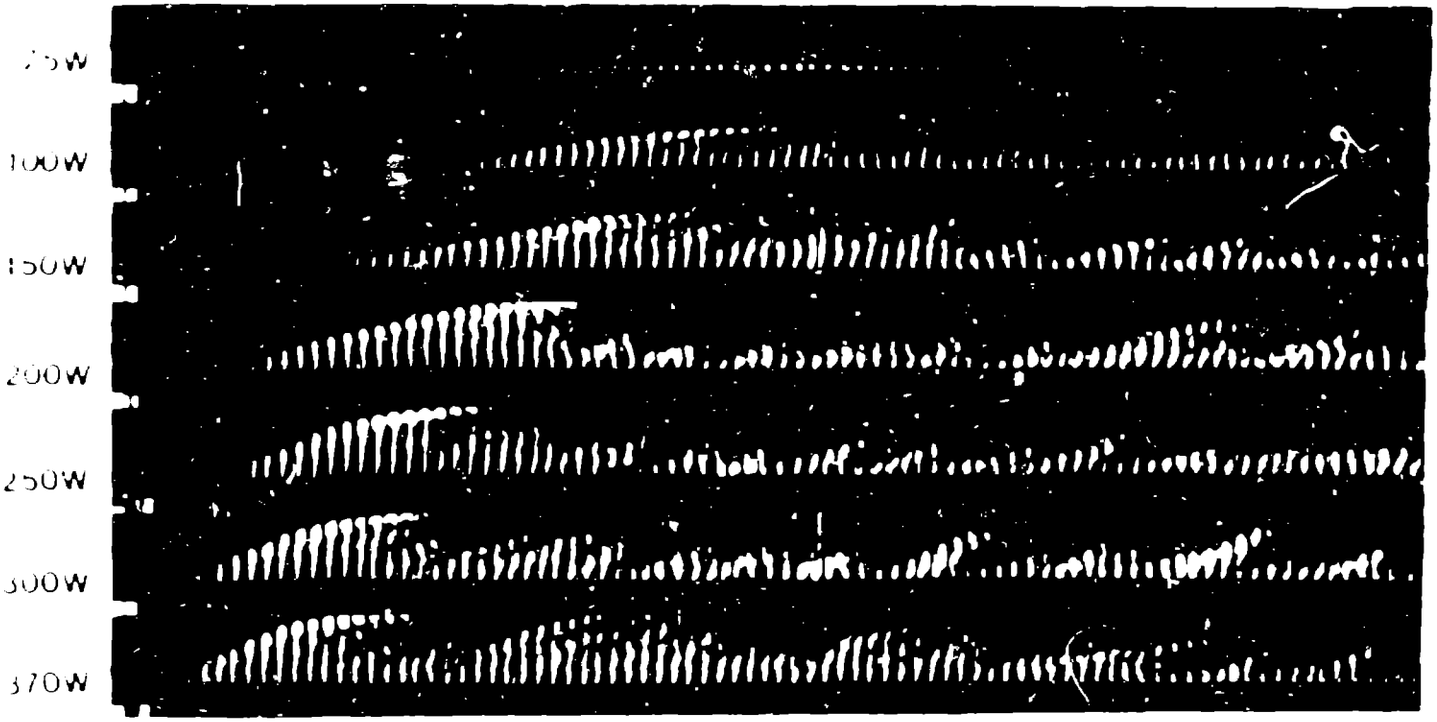

1100Al (7ms, 10pps)

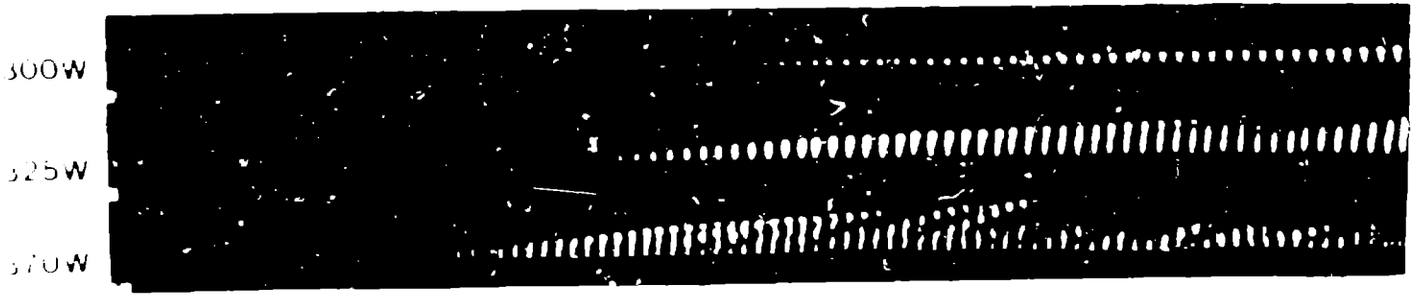

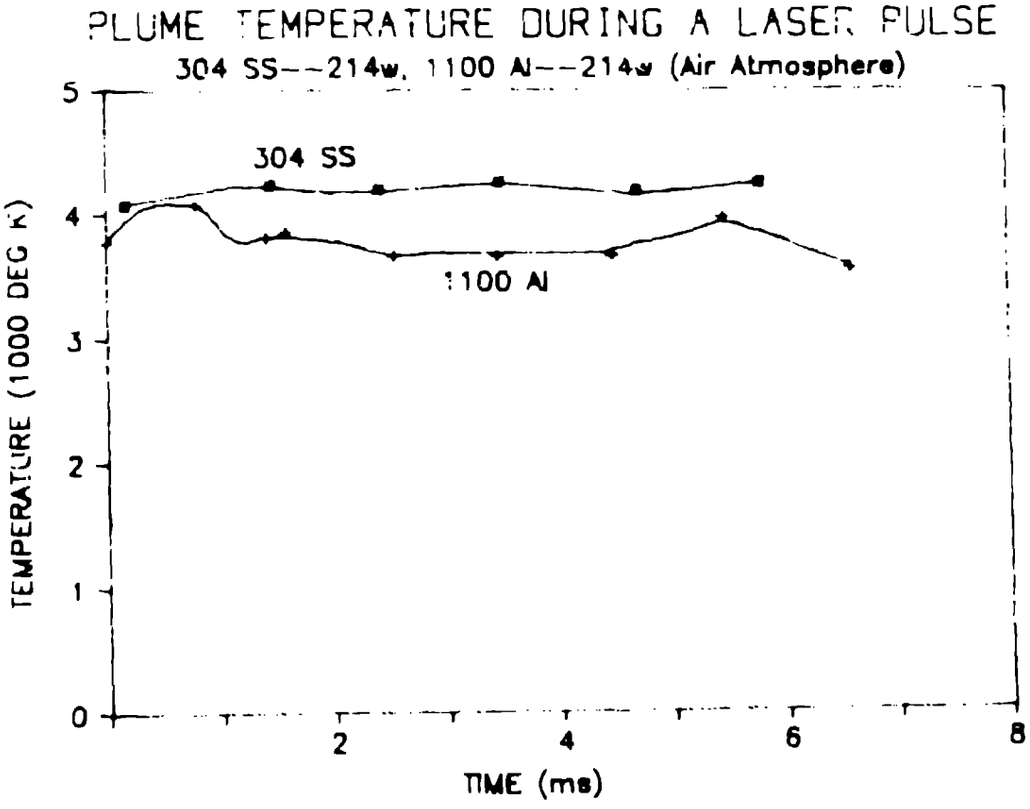
PLUME TEMPERATURE DURING A LASER PULSE
304 SS--214w, 1100 Al--214w (Air Atmosphere)
304 SS
1100 Al
TEMPERATURE (1000 DEG K)
TIME (ms)
0
1
2
3
4
5
2
4
6
8

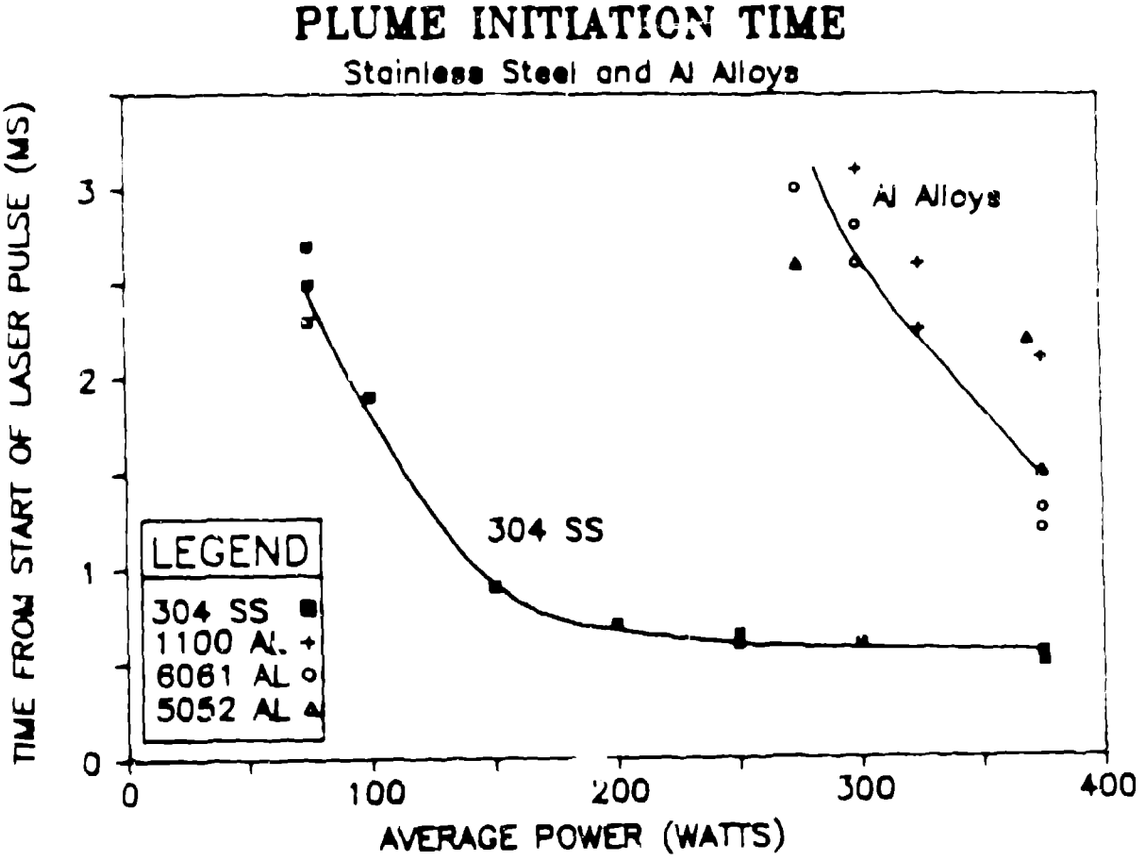
PLUME INITIATION TIME
Stainless Steel and Al Alloys
TIME FROM START OF LASER PULSE (MS)
AVERAGE POWER (WATTS)
0
1
2
3
0
100
200
300
400
Al Alloys
304 SS
LEGEND
304 SS
1100 AL.
6061 AL
5052 AL

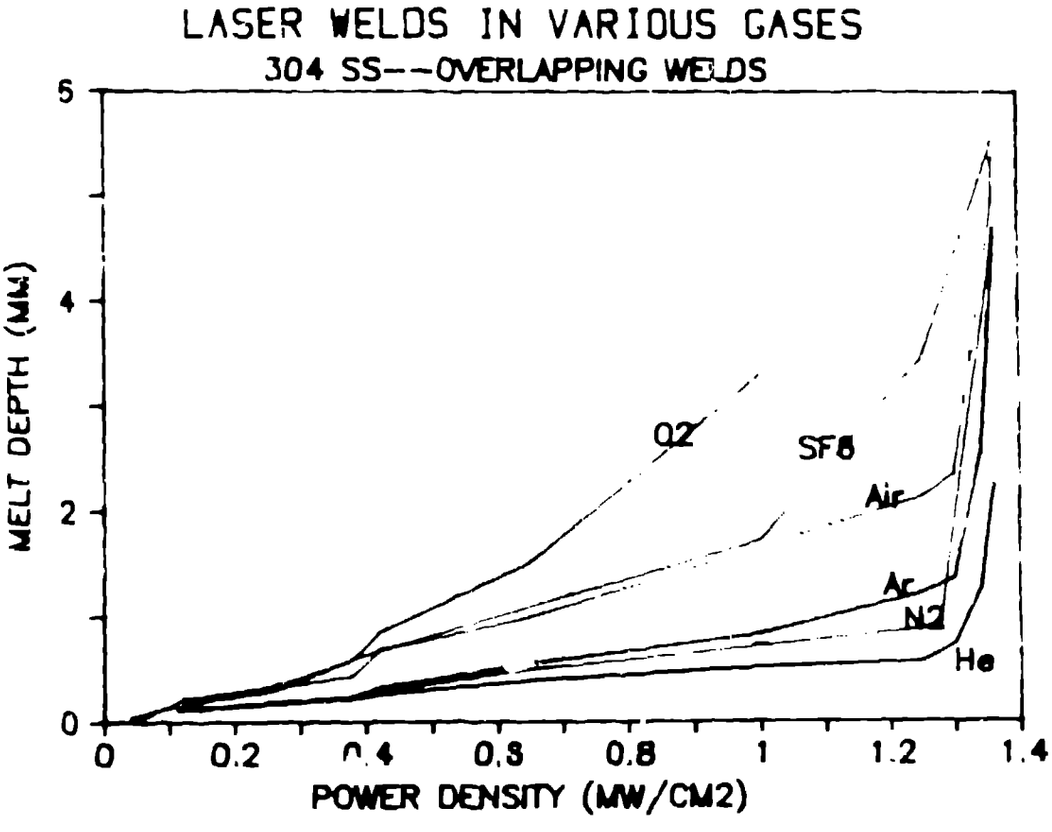
LASER WELDS IN VARIOUS GASES
304 SS--OVERLAPPING WELDS
MELT DEPTH (MM)
POWER DENSITY (MW/CM2)
0
2
4
6
0
0.2
0.4
0.6
0.8
1
1.2
1.4
O2
SF6
Air
Ar
N2
He

Figure 10

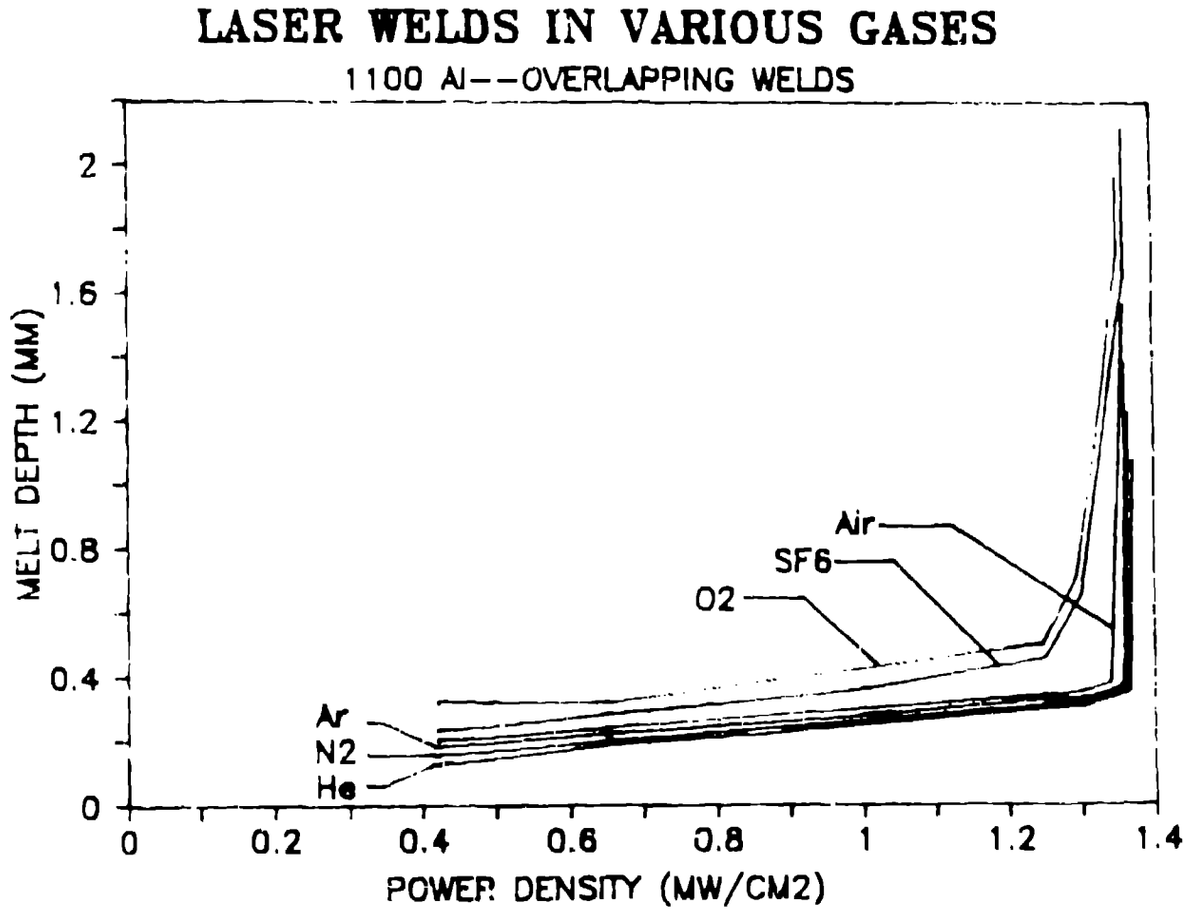
LASER WELDS IN VARIOUS GASES
1100 Al--OVERLAPPING WELDS
MELT DEPTH (MM)
2
1.6
1.2
0.8
0.4
0
Air
SF6
O2
Ar
N2
He
0
0.2
0.4
0.6
0.8
1
1.2
1.4
POWER DENSITY (MW/CM2)

Figure 11

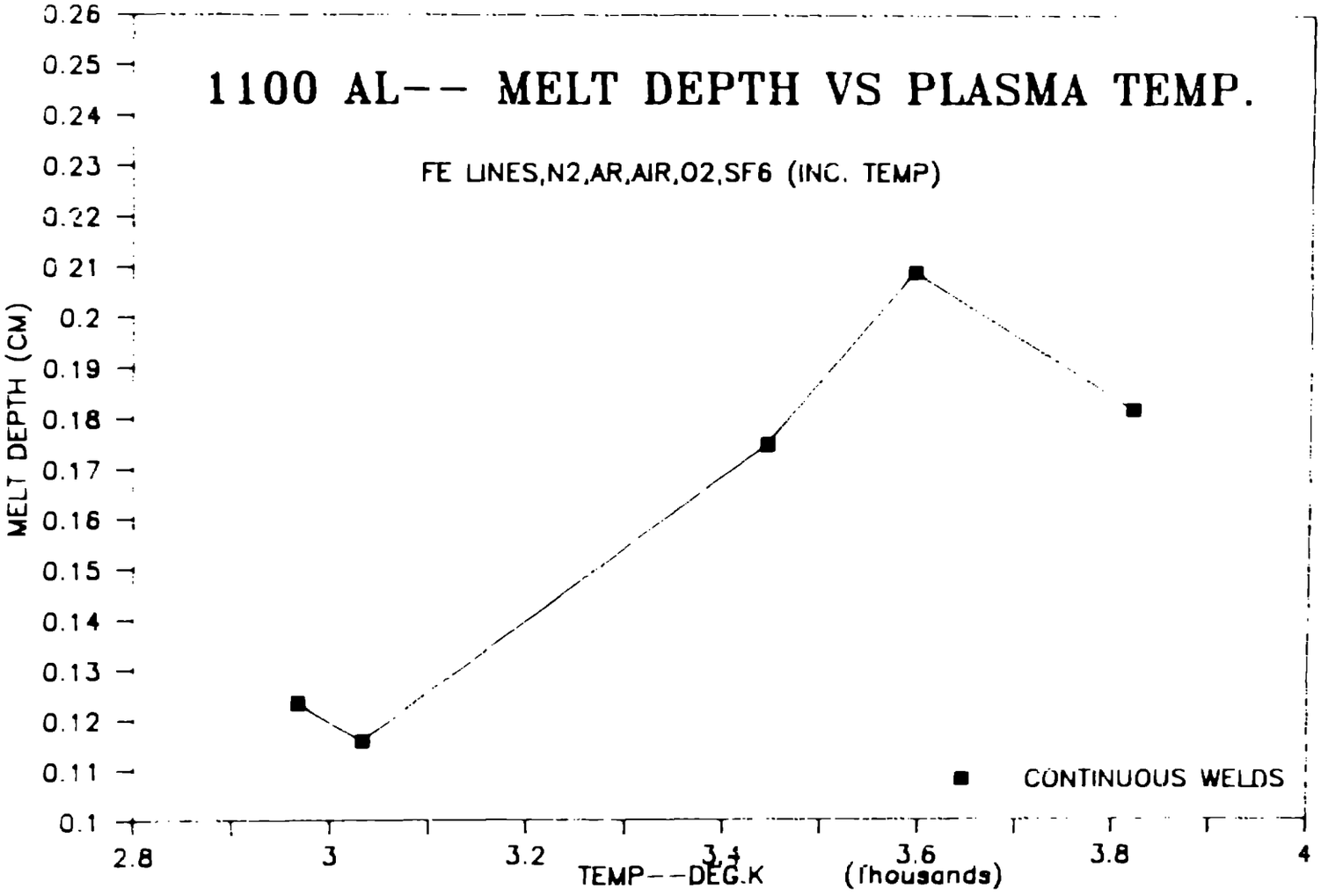
1100 AL-- MELT DEPTH VS PLASMA TEMP.
FE LINES,N2,AR,AIR,O2,SF6 (INC. TEMP)
MELT DEPTH (CM)
0.26
0.25
0.24
0.23
0.22
0.21
0.2
0.19
0.18
0.17
0.16
0.15
0.14
0.13
0.12
0.11
0.1
2.8
3
3.2
3.4
3.6
3.8
4
TEMP--DEG.K
(Thousands)
CONTINUOUS WELDS

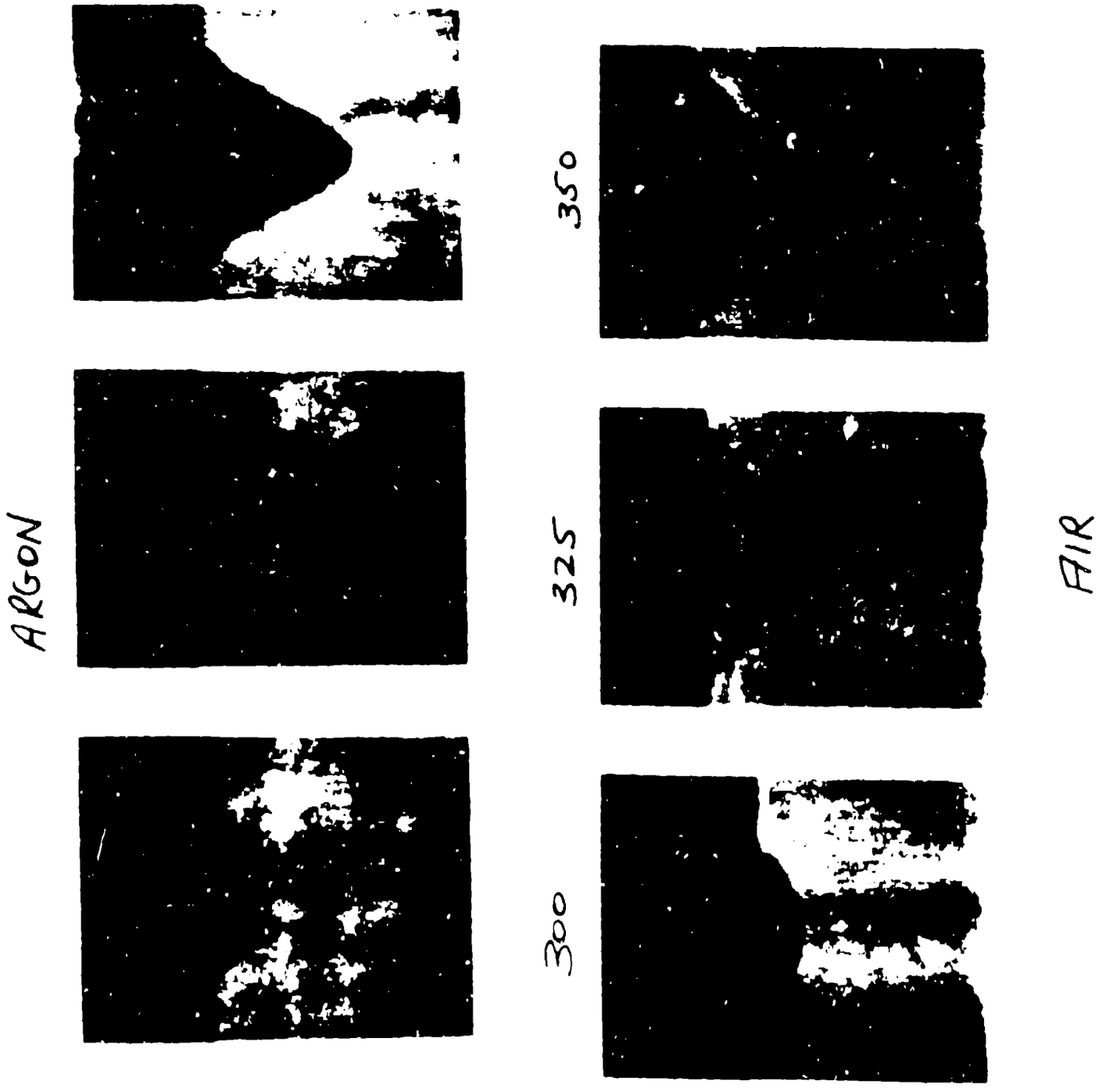

Figure 11